Determination of the Spin-Rotation Fine Structure of He_2^+

Paul Jansen, Luca Semeria, and Frédéric Merkt*
Laboratory of Physical Chemistry, ETH Zurich, CH-8093 Zurich, Switzerland

(Received 13 October 2017; published 26 January 2018)

Measuring spin-rotation intervals in molecular cations is challenging, particularly so when the ions do not have electric-dipole-allowed rovibrational transitions. We present a method, based on an angular-momentum basis transformation, to determine the spin-rotational fine structure of molecular ions from the fine structure of high Rydberg states. The method is illustrated by the determination of the so far unknown spin-rotation fine structure of the fundamentally important He_2^+ ion in the $X\ ^2\Sigma_u^+$ state. The fine-structure splittings of the $v^+ = 0$, $N^+ = 1$, 3, and 5 levels of He_2^+ are 7.96(14), 17.91(32), and 28.0(6) MHz, respectively. The experiment relies on the use of single-mode cw radiation to record spectra of high Rydberg states of He_2 from the $a\ ^3\Sigma_u^+$ metastable state.

DOI: 10.1103/PhysRevLett.120.043001

He_2^+ is a structurally simple molecular system and was one of the first molecules to be studied by *ab initio* quantum-mechanical methods [1,2]. Its $X\ ^2\Sigma_u^+$ electronic ground state has the electronic configuration $(1\sigma_g)^2(1\sigma_u)^1$, with two electrons in the $1\sigma_g$ bonding orbital and one electron in the antibonding $1\sigma_u$ orbital. Its dissociation energy $D_0(^4He_2^+)/hc$ and equilibrium internuclear separation R_e are 19116.116 cm^{-1} and $2.042a_0$, respectively [3,4]. He_2^+ is encountered in He-containing plasmas [5], is a central structural element in positively charged helium clusters [6], and is thought to have been one of the first molecules formed in the early Universe [7].

The small charge of the He nuclei and the small number of electrons make He_2^+ one of the few molecules, next to H_2^+, H_2, HHe^+, LiH^+, and LiH, for which exact quantum-mechanical computations are, in principle, possible (see, e.g., Refs. [4,8–10]). The comparison of the results of such computations with the results of spectroscopic measurements offers the prospects of either identifying incomplete aspects of the theoretical treatment or uncovering new effects. The rapidly growing efforts invested in such comparisons are part of the search for what is referred to as "physics beyond the standard model" using molecules [11,12]. Such searches exploit molecular systems to attempt, e.g., the observation of so far unknown forces [13] or of compactified higher dimensions [14]. Precision spectroscopy in simple few-electron molecules may also contribute to resolve what is known as the proton-charge-radius puzzle [15,16]. A crucial aspect of these efforts is the establishment and testing of reliable and highly accurate computational procedures, which is best done with the simplest molecules.

Until recently, the experimental data available on the energy-level structure of He_2^+ consisted of only 16 transitions [17–19]: nine rovibrational transitions in the IR connecting rotational levels of the ground ($v = 0$) and first excited ($v = 1$) vibrational level of $^3He^4He^+$ [17,18], which, unlike $^4He_2^+$, possesses a permanent electric dipole moment, and seven electronic transitions in the microwave range connecting weakly bound rovibrational levels of the $X\ ^2\Sigma_u^+$ and $A\ ^2\Sigma_g^+$ electronic states of $^4He_2^+$ [19]. These data could be fully accounted for by the latest *ab initio* calculations [4]. They have since been extended by precision measurements of the positions of many rotational levels of the ground vibronic state of $^4He_2^+$, which revealed systematic and increasing deviations between calculated and experimental energies with increasing rotational excitation [20–23].

No information has been obtained so far on the spin-rotation splittings of the He_2^+ rotational levels. Yu, Wing, and Adamowicz [18] could measure the hyperfine structure in the IR spectrum of $^3He^4He^+$ arising from the $I = 1/2$ nuclear spin of ^3He but did not resolve the spin-rotation splittings. A calculation of the spin-rotation interaction indicated a spin-rotation coupling constant $\gamma^+(^3He^4He^+)$ of about −3.5 MHz [18], too small to be observed in the IR spectra. Taking the μ^{-1} dependence of the spin-rotation coupling constant on the reduced mass μ, a value of about −3 MHz can be predicted for $\gamma^+(^4He_2^+)$, more than 10 times less than in the ground state of H_2^+ [24–26]. The contribution to the spin-rotation constant from the second-order spin-orbit coupling [27,28] is small in He_2^+ because of the large energetic separation of the ground state from excited electronic states. From a precision measurement of the spin-rotation intervals, one may determine the frequencies of the radio-wave magnetic transitions between the spin-rotation components, through which He_2^+ might be detected.

We demonstrate here a method to determine the spin-rotation splittings of the rotational levels of molecular cations from the fine structure of high Rydberg states and illustrate it by a measurement of the spin-rotation splittings of He_2^+. Their small size necessitates the use of

narrow-band cw laser radiation to record the Rydberg spectrum at high values of the principal quantum number, which, to our knowledge, has not yet been possible in any molecular system.

We recorded the Rydberg spectrum of He_2 from the metastable a $^3\Sigma_u^+$ state (He_2^* hereafter) in a supersonic beam [29] using the spectrometer described in Ref. [30]. The single-mode cw UV laser radiation (bandwidth 2 MHz, power 300 mW) used to record the spectrum was generated by frequency doubling the output of a ring dye laser in a nonlinear crystal placed in an enhancement cavity. The perpendicular arrangement of the He_2^* and UV-laser beams reduced the Doppler width to 25 MHz and the precision of the fine-structure intervals to about 2.5 MHz [30]. Transitions were detected by the delayed pulsed-field ionization of the Rydberg states. Spectra of selected transitions are depicted in Fig. 2. Most of the measurements were carried out at n values around 50 except for weak series, for which measurements had to be performed at $n \approx 30$, and for strong series, for which measurements could also be performed at n values up to 100.

Because the total molecular wave function must be symmetric under an exchange of the spinless bosonic $^4He^{2+}$ nuclei, only odd rotational levels exist in He_2^* and in the $X\,^2\Sigma_u^+$ electronic ground state of He_2^+. In the following, double-prime symbols, unprimed symbols, and a superscript "+" are used to designate the quantum numbers of He_2^*, He_2 Rydberg states, and He_2^+, respectively. The level structure of He_2^* is best described using Hund's angular-momentum coupling case (b), where the total angular momentum excluding spin $\vec{N}''$ couples to the total electron spin $\vec{S}''$ to form the total angular momentum $\vec{J}''$. The spin-spin and spin-rotation interaction split each rotational level into three components with $J'' = N''$, $N'' \pm 1$. The characteristic spacing of the resulting fine structure of He_2^* has been measured for several rovibrational levels [31–35] and is dominated by the spin-spin interaction, which is two orders of magnitude stronger than the spin-rotation interaction [35]. The level structure of the $X\,^2\Sigma_u^+(v^+ = 0)$ state of He_2^+ is also best described using Hund's case (b). The rotational levels are split into two fine-structure components by

$$\tilde{\nu}_{\mathrm{sr}}^+ = \gamma_{N^+}^+ \left(N^+ + \frac{1}{2}\right), \quad \text{with} \quad \gamma_{N^+}^+ = \gamma^+ + \gamma_D^+ N^+(N^+ + 1). \tag{1}$$

In the absence of ℓ mixing, the angular-momentum coupling scheme of the Rydberg states of He_2 depends on the relative strength of five competing interactions: (i) the exchange interaction between Rydberg and core electrons, (ii) the spin-rotation interaction of the ion core, (iii) the spin-spin interaction, (iv) the spin-orbit interaction, and (v) the ℓ-uncoupling interaction that is responsible for the transition from Hund's case (b) to case (d) [36,37] and is complete for $n \gtrsim 10$. Because of the small nuclear charge of He, the spin-orbit interaction is completely negligible. The spin-spin interaction scales as n^{-3} and is negligible in Rydberg states with $n > 10$. The interactions that are responsible for the level structure in the Rydberg states of He_2 are the spin-rotation interaction of the ion core, which is n independent, and the exchange interaction, which splits the np Rydberg states in a singlet and a triplet state by

$$\Delta E_{\mathrm{ex}} \approx \Delta\delta^{(S,T)} \frac{2hc\mathcal{R}_{\mathrm{He_2}}}{n^3}, \tag{2}$$

where $\Delta\delta^{(S,T)}$ is the difference between the Hund's case (d) quantum defects, $\delta_{N,S}$, of the singlet and triplet states and $\mathcal{R}_{\mathrm{He_2}}$ is the mass-corrected Rydberg constant for He_2. Taking γ^+ from Yu, Wing, and Adamowicz [18] and estimating $\Delta\delta^{(S,T)}$ from the *ab initio* potential curves of Yarkony [38], Eqs. (1) and (2) predict that the spin-rotation interaction in the core is much less than the exchange interaction in Rydberg states with $n < 150$, so that the total electron spin S is a good quantum number in this range. The Rydberg states are adequately described in Hund's case (d), where $\vec{N}^+$ couples to $\vec{\ell}$ to form $\vec{N}$, which couples to $\vec{S}$ to give $\vec{J}$ [see Fig. 1(a)]. Above about $n = 150$, $\vec{N}^+$ couples to the spin of the core $\vec{S}^+$, which mixes singlet and triplet states [39], to form $\vec{J}^+$, $\vec{\ell}$ couples to the spin of the Rydberg electron $\vec{s}$, and the resulting vector $\vec{j}$ couples to $\vec{J}^+$ to form $\vec{J}$. This situation corresponds to Hund's case (e[b]), depicted in Fig. 1(b). When n approaches infinity, the different J levels originating from the same J^+ value are split by the spin-rotation intervals of the ion levels. The Rydberg transitions observed in our spectra connect the Hund's case (b) levels of He_2^* to the Hund's case (d) Rydberg levels and can be labeled as $npN_{N,J}^+ \leftarrow N''_{J''}$.

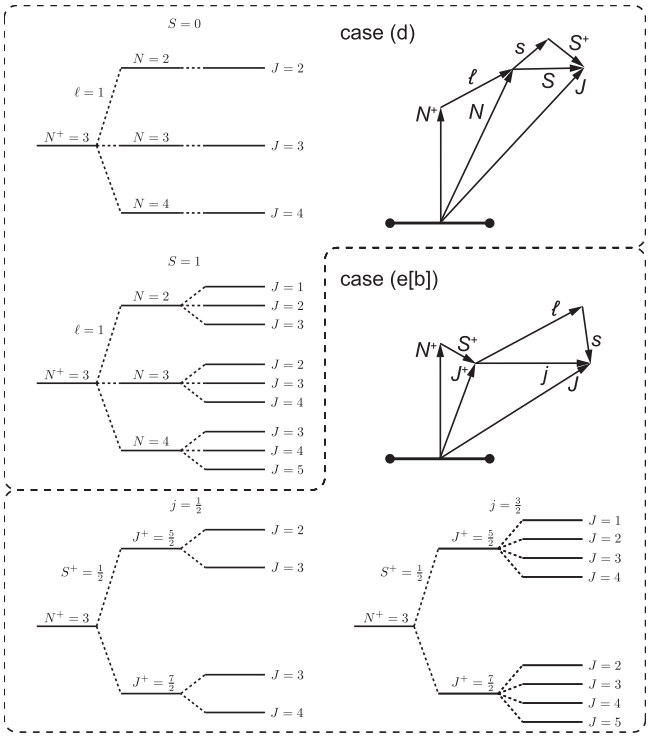

FIG. 1. Hund's coupling cases (d) and (e[b]) and the corresponding level structure (not to scale) of high Rydberg states of He_2.

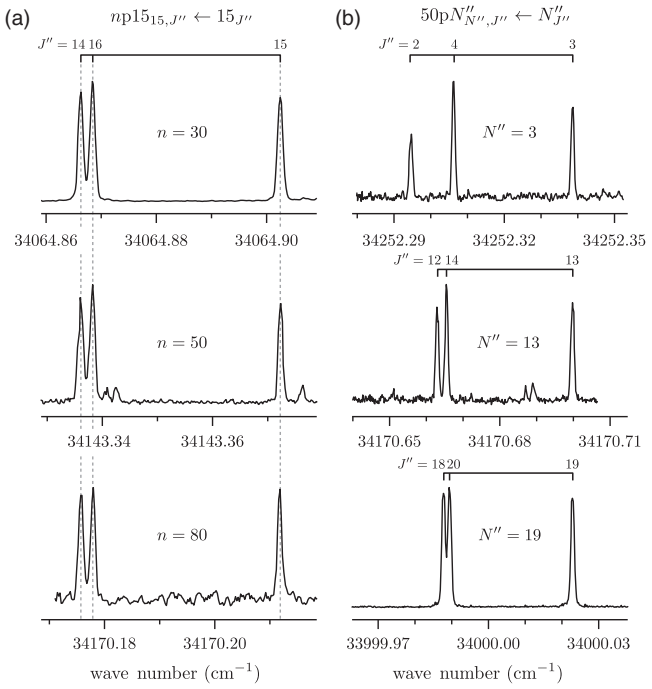

FIG. 2. (a) Rydberg spectra of $np15_{15} \leftarrow 15$ transitions with $n = 30$, 50, and 80. (b) Spectra of $50pN''_{N''} \leftarrow N''$ with $N'' = 3$, 13, and 19. See the text for details.

Hund's case (d), $|N^+NS\rangle = |NS\rangle$, and Hund's case (e[b]), $|N^+J^+j\rangle = |J^+j\rangle$, basis functions, as defined in Ref. [40], are related by the angular-momentum basis transformation

$$\mathcal{U} \equiv \langle J^+ j | NS \rangle^{(JM_J p \Lambda^+ N^+ S^+ q^+ \ell s)} = \sqrt{(2j+1)(2J^++1)(2S+1)(2N+1)} \times \left(\frac{1+\delta_{\Lambda^+0}(-1)^{p-q^+-N^++\ell}}{1+\delta_{\Lambda^+0}} \right) \begin{Bmatrix} N^+ & S^+ & J^+ \\ \ell & s & j \\ N & S & J \end{Bmatrix}, \quad (3)$$

where $q^+ = 0$ and $p = 1$ are the electronic core and total parity indices, respectively, $\Lambda^+ = 0$, and the last term is a Wigner-9j symbol. Equation (3) can be derived from the diagrams presented in Fig. 1 using standard angular-momentum algebra (see, e.g., Ref. [41]). The fine structure of the np Rydberg states of He_2 for each set of n and N^+ values is derived from the eigenvalues of the 12×12 matrix

$$\hat{\mathcal{H}} = \hat{\mathcal{H}}_{n,N^+,N,S} + \mathcal{U}^\dagger \hat{\mathcal{H}}^+_{\rm sr} \mathcal{U}, \quad (4)$$

where $\hat{\mathcal{H}}_{n,N^+,N,S}$ is a diagonal matrix describing the Hund's case (d) limit, with three sets of four elements for each value of N ($N = N^+$, $N^+ \pm 1$): three degenerate elements corresponding to the triplet manifold ($S = 1$) and one to the singlet manifold ($S = 0$). Neglecting channel interactions, the diagonal elements are given by

$$E_{n,N^+,N,S} = E_{N^+} - \frac{hc\mathcal{R}_{\rm He_2}}{(n-\delta_{N,S})^2}. \quad (5)$$

$\hat{\mathcal{H}}^+_{\rm sr}$ is expressed in the Hund's case (e[b]) limit as a diagonal matrix with two sets of six degenerate elements, $\frac{1}{2}hc\gamma^+_{N^+}N^+$ and $-\frac{1}{2}hc\gamma^+_{N^+}(N^++1)$, corresponding to the spin-rotation fine structure of the ion. A similar procedure has been used previously in the context of the case (b) to case (d) frame transformation and the rotational structure of NO^+ [42] and CaF^+ [43]. Because the splittings of $n < 150$ Rydberg states of different N and S values are much larger than the spin-rotation splitting of the ion, except near perturbations arising from channel interactions, the eigenvalues of Eq. (4) do not depend on n or on the quantum defects $\delta_{N,S}$. The relation between the fine-structure intervals in the Rydberg states and the ion is thus *purely geometrical* and given by Eqs. (1), (3), and (4). This is illustrated in Fig. 2(a), which compares the fine structure of the spectra of the $np15_{15} \leftarrow 15$ for $n = 30$, 50, and 80. Figure 2(b) shows how the fine structure evolves with the value of N''. Analytic expressions for the fine-structure splittings of the Rydberg states resulting from Eqs. (1)–(5) are given in Table I. Compared to an extrapolation of the ionic fine structure by multichannel quantum-defect theory (MQDT), Eqs. (3) and (4) offer the advantage that they do not require knowledge of the quantum defects.

Transitions from He_2^* to np Rydberg states are governed by selection rules. The transition electric dipole moment does not act on the spins, so that in this case $\Delta J = J - J'' = N - N'' = \Delta N$. The allowed transitions are depicted in Fig. 3 for $N'' = 3$. Their transition frequencies depend on the fine structures of both the metastable state and the Rydberg state. Because the fine-structure splittings of the metastable state are precisely known [31–35,44], the fine structure of the Rydberg states can be reconstructed in a straightforward manner, as illustrated in Fig. 4. The diamonds in Fig. 4(a) give the relative positions of the three lines observed experimentally (see the

TABLE I. Spin-rotation intervals of high np Rydberg states as a function the spin-rotation coupling constant γ^+ of the $X\ ^2\Sigma^+_u$ ion core.

N	$J = N-1$	$J = N$	$J = N+1$
$N^+ - 1$	0	$\gamma^+ N(N+2)/(2(N+1))$	$\gamma^+(2N+1)(N+2)/(2(N+1))$
N^+	0	$\gamma^+(N^2+N-1)/(2(N+1))$	$\gamma^+(N^2+N-1)(2N+1)/(2N(N+1))$
$N^+ + 1$	0	$\gamma^+(N-1)/2$	$\gamma^+(2N+1)(N-1)/(2N)$

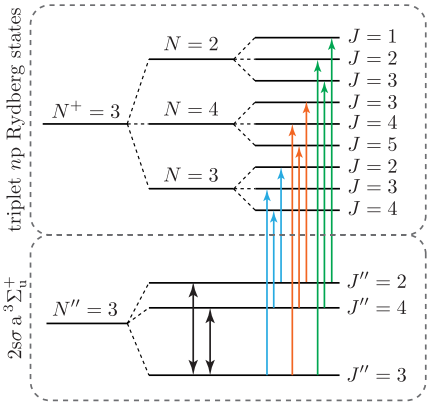

FIG. 3. Illustration of the $\Delta J = \Delta N$ selection rule for Rydberg transitions from $N'' = 3$. The double-headed arrows indicate the fine-structure splittings in He_2^*.

examples in Fig. 2). The dashed lines correspond to the fine-structure intervals in the metastable state, and the differences indicated by the shaded regions represent the fine structure of the Rydberg states, which are listed in Table II. This structure is compared in Fig. 4(b) with the fine structure derived from the eigenvalues of Eq. (4) after optimizing the values of γ^+ [best value $-5.14(9)$ MHz] and γ_D^+ [best value 1.30(17) kHz] in a nonlinear least-squares fit (solid lines). The fine-structure intervals calculated with these constants are also compared to the experimentally determined intervals in Table II. The deviations exceed 5 MHz in only four cases. The reduced-χ_ν^2 value of the fit is 1.05, indicating that our model describes the experimental data well. We also performed a MQDT analysis of the

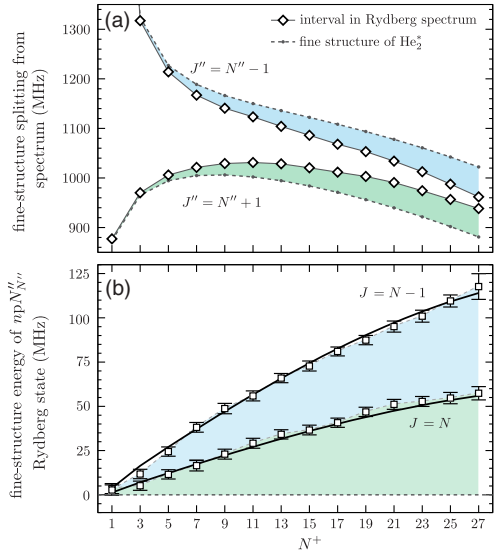

FIG. 4. (a) Fine-structure components, relative to the $J'' = N''$ component, of Rydberg spectra recorded from He_2^*, as a function of N^+ (diamonds) and fine-structure intervals of He_2^* (dashed lines) [31–35,44]. The green and blue shaded regions indicate the spin-rotation fine structure of the Rydberg states. (b) Extracted fine structure of Rydberg states relative to the $J'' = N'' + 1$ component (squares) compared to model calculations (solid lines).

Rydberg spectrum using the methodology and program developed by Jungen and co-workers [37] and including the spins following the procedure described for H_2 in Refs. [26,39], but with the quantum-defect parameters obtained for the triplet states of He_2 in Ref. [21]. The analysis included the ℓ-mixing interaction between p and f triplet Rydberg states of He_2, first observed at $n = 4$ in Ref. [45]. Such interactions scale as n^{-3}, lead to level shifts that are much less than the widths of the lines observed in our spectra at $n = 50$, and tend to affect all fine-structure components in the same way. This analysis led to γ^+ and γ_D^+ values of $-5.04(9)$ and 1.22(17) kHz, respectively, in perfect agreement with the results obtained with Eq. (4). With γ^+ and γ_D^+, the frequencies of the magnetic-dipole

TABLE II. Experimental fine-structure intervals of triplet np Rydberg states of He_2 (ν_{obs}) and their comparison to the results of our model calculations ($\Delta = \nu_{obs} - \nu_{calc}$). All values are given in megahertz.

	$J = N \leftarrow J = N + 1$		$J = N \leftarrow J = N - 1$	
npN_N^+	ν_{obs}	Δ	ν_{obs}	Δ
$27p1_1$	2(8)	1.3	3(3)	1.5
$49p1_1$	4(3)	−1.1	−1(3)	−2.1
$50p3_3$	5(3)	−4.7	7(3)	−0.4
$41p3_4$	10(3)	3.8	11(3)	3.7
$98p3_4$	8(4)	3.6	13(5)	4.9
$99p3_4$	14(3)	1.8	5(3)	−2.9
$101p3_4$	16 (4)	9.9	11(4)	3.1
$50p5_5$	11(3)	−2.7	13(3)	0.6
$44p5_6$	11 (3)	3.4	20(3)	7.3
$50p7_7$	17(3)	0.9	22(3)	4.2
$50p7_8$	24(3)	−0.1	14(3)	−3.9
$32p9_9$	23(3)	1.6	25(3)	3.1
$50p9_9$	23(3)	1.6	25.7(15)	3.4
$63p9_9$	26(3)	1.3	22.4(19)	0.1
$63p9_{10}$	25(4)	3.1	26(4)	3.2
$50p11_{11}$	29(3)	−0.7	27(3)	−0.3
$35p11_{12}$	32(3)	−1.0	24(3)	−3.5
$50p13_{13}$	34(3)	0.2	32(3)	0.1
$54p13_{13}$	27.6(25)	−2.5	36(3)	4.0
$54p13_{14}$	41(3)	1.2	26(3)	−6.1
$30p15_{15}$	36(3)	−0.7	38(3)	1.7
$50p15_{15}$	37(3)	−1.6	36(3)	0.2
$54p15_{15}$	37(3)	−3.1	35(3)	−1.3
$54p15_{16}$	32.7(25)	−1.5	40.4(25)	4.2
$55p15_{15}$	34(4)	−0.7	40(5)	4.0
$55p15_{16}$	42(3)	1.5	31(4)	−4.8
$80p15_{15}$	32(3)	0.8	43(3)	6.7
$80p15_{16}$	35.7(17)	−0.6	38(3)	2.1
$30p17_{17}$	41(3)	−1.6	40.3(25)	0.1
$91p17_{17}$	37(11)	−1.6	44(11)	4.0
$91p17_{18}$	41(3)	−0.2	41(3)	0.9
$30p19_{19}$	47(3)	−2.8	41(3)	−3.4
$30p21_{21}$	51(3)	−2.2	44(3)	−3.5
$30p23_{23}$	53(3)	−2.7	48(3)	−2.5
$30p25_{25}$	55(3)	0.3	55(3)	1.3
$30p27_{27}$	57(4)	3.7	60(7)	4.3

TABLE III. Predicted frequencies of magnetic-dipole transitions of $He_2^+(X\,^2\Sigma_u^+, v^+ = 0)$.

$N^+(J^{+\prime}) \leftarrow N^+(J^{+\prime\prime})$	Frequency (MHz)
$1(1/2) \leftarrow 1(3/2)$	7.69(14)
$3(5/2) \leftarrow 3(7/2)$	17.91(32)
$5(9/2) \leftarrow 5(11/2)$	28.0(6)

transitions connecting the fine-structure levels of the lowest rotational states of He_2^+ that are expected to be the most relevant for astrophysics are predicted with an accuracy of better than 1 MHz (see Table III).

We have demonstrated a new method to precisely measure fine-structure intervals in molecular ions and showed how they are related to the fine structure of the corresponding Rydberg states. Applying this method to He_2^+, we determined the spin-rotation fine structure of the ground vibronic state for the first time. The spin-rotation coupling constant significantly differs from the value derived by scaling the value calculated *ab initio* for $^3He^4He^+$ [18] (see above). When combined with the rotational term values of the $X\,^2\Sigma_u^+(v^+ = 0)$ state of He_2^+ reported in Ref. [23], the present data provide the complete level structure of the vibronic ground state of He_2^+.

We thank H. Schmutz and J. A. Agner for technical assistance and M. Beyer for useful discussions. This work was supported by the Swiss National Science Foundation (Grant No. 200020-172620) and by the European Research Council (Horizon 2020, Advanced Grant No. 743121).

*merkt@xuv.phys.chem.ethz.ch

[1] E. Majorana, Nuovo Cimento **8**, 22 (1931).
[2] L. Pauling, J. Chem. Phys. **1**, 56 (1933).
[3] J. Xie, B. Poirier, and G. I. Gellene, J. Chem. Phys. **122**, 184310 (2005).
[4] W.-C. Tung, M. Pavanello, and L. Adamowicz, J. Chem. Phys. **136**, 104309 (2012).
[5] C. B. Collins and W. W. Robertson, J. Chem. Phys. **40**, 2208 (1964).
[6] B. E. Callicoatt, K. Förde, L. F. Jung, T. Ruchti, and K. C. Janda, J. Chem. Phys. **109**, 10195 (1998).
[7] S. Lepp, P. C. Stancil, and A. Dalgarno, J. Phys. B **35**, R57 (2002).
[8] V. I. Korobov, L. Hilico, and J.-P. Karr, Phys. Rev. A **89**, 032511 (2014).
[9] K. Piszczatowski, G. Łach, M. Przybytek, J. Komasa, K. Pachucki, and B. Jeziorski, J. Chem. Theory Comput. **5**, 3039 (2009).
[10] M. Puchalski, J. Komasa, P. Czachorowski, and K. Pachucki, Phys. Rev. Lett. **117**, 263002 (2016).
[11] T. Steimle and W. Ubachs, J. Mol. Spectrosc. **300**, 1 (2014).
[12] W. Ubachs, J. C. J. Koelemeij, K. S. E. Eikema, and E. J. Salumbides, J. Mol. Spectrosc. **320**, 1 (2016).
[13] E. J. Salumbides, J. C. J. Koelemeij, J. Komasa, K. Pachucki, K. S. E. Eikema, and W. Ubachs, Phys. Rev. D **87**, 112008 (2013).
[14] E. J. Salumbides, A. N. Schellekens, B. Gato-Rivera, and W. Ubachs, New J. Phys. **17**, 033015 (2015).
[15] A. Antognini *et al.*, Science **339**, 417 (2013).
[16] R. Pohl *et al.*, Science **353**, 669 (2016).
[17] N. Yu and W. H. Wing, Phys. Rev. Lett. **59**, 2055 (1987).
[18] N. Yu, W. H. Wing, and L. Adamowicz, Phys. Rev. Lett. **62**, 253 (1989).
[19] A. Carrington, C. H. Pyne, and P. J. Knowles, J. Chem. Phys. **102**, 5979 (1995).
[20] M. Raunhardt, M. Schäfer, N. Vanhaecke, and F. Merkt, J. Chem. Phys. **128**, 164310 (2008).
[21] D. Sprecher, J. Liu, T. Krähenmann, M. Schäfer, and F. Merkt, J. Chem. Phys. **140**, 064304 (2014).
[22] P. Jansen, L. Semeria, L. E. Hofer, S. Scheidegger, J. A. Agner, H. Schmutz, and F. Merkt, Phys. Rev. Lett. **115**, 133202 (2015).
[23] L. Semeria, P. Jansen, and F. Merkt, J. Chem. Phys. **145**, 204301 (2016).
[24] K. B. Jefferts, Phys. Rev. Lett. **23**, 1476 (1969).
[25] Z. W. Fu, E. A. Hessels, and S. R. Lundeen, Phys. Rev. A **46**, R5313 (1992).
[26] A. Osterwalder, A. Wüest, F. Merkt, and C. Jungen, J. Chem. Phys. **121**, 11810 (2004).
[27] J. M. Brown and A. Carrington, *Rotational Spectroscopy of Diatomic Molecules* (Cambridge University Press, Cambridge, England, 2003).
[28] H. Lefebvre-Brion and R. W. Field, *The Spectra and Dynamics of Diatomic Molecules* (Academic Press, San Diego, 2004).
[29] M. Motsch, P. Jansen, J. A. Agner, H. Schmutz, and F. Merkt, Phys. Rev. A **89**, 043420 (2014).
[30] P. Jansen, L. Semeria, and F. Merkt, J. Mol. Spectrosc. **322**, 9 (2016).
[31] W. Lichten, M. V. McCusker, and T. L. Vierima, J. Chem. Phys. **61**, 2200 (1974).
[32] W. Lichten and T. Wik, J. Chem. Phys. **69**, 98 (1978).
[33] M. Kristensen and N. Bjerre, J. Chem. Phys. **93**, 983 (1990).
[34] I. Hazell, A. Norregaard, and N. Bjerre, J. Mol. Spectrosc. **172**, 135 (1995).
[35] C. Focsa, P. F. Bernath, and R. Colin, J. Mol. Spectrosc. **191**, 209 (1998).
[36] U. Fano, Phys. Rev. A **2**, 353 (1970).
[37] C. Jungen, Elements of Quantum Defect Theory, in *Handbook of High-Resolution Spectroscopy*, edited by M. Quack and F. Merkt, Vol. 1 (Wiley, New York, 2011).
[38] D. R. Yarkony, J. Chem. Phys. **90**, 7164 (1989).
[39] C. Haase, M. Beyer, C. Jungen, and F. Merkt, J. Chem. Phys. **142**, 064310 (2015).
[40] C. Jungen and G. Raseev, Phys. Rev. A **57**, 2407 (1998).
[41] R. N. Zare, *Angular Momentum: Understanding Spatial Aspects in Chemistry and Physics* (Wiley, New York, 1988).
[42] S. Fredin, D. Gauyacq, M. Horani, C. Jungen, G. Lefevre, and F. Masnou-Seeuws, Mol. Phys. **60**, 825 (1987).
[43] R. W. Field, C. M. Gittins, N. A. Harris, and C. Jungen, J. Chem. Phys. **122**, 184314 (2005).
[44] L. Semeria, P. Jansen, J. A. Agner, H. Schmutz, and F. Merkt (unpublished).
[45] G. Herzberg and C. Jungen, J. Chem. Phys. **84**, 1181 (1986).